Proceedings of *The Riddle of Cooling Flows in Galaxies and Clusters of Galaxies*
May 31 – June 4, 2003, Charlottesville, Virginia, USA
Ed. T. H. Reiprich, J. C. Kempner, & N. Soker

Magnetic fields and cosmic rays in galaxy cluster cooling flows

Torsten Enßlin, Corina Vogt, and Christoph Pfrommer

Max-Planck-Institut für Astrophysik, Karl-Schwarzschild-Str. 1, 85741 Garching, Germany

Cooling flows are regions where the importance of non-thermal intra-cluster medium components such as magnetic fields and cosmic rays may be strongest within a galaxy cluster. They are also regions where such components are best detectable due to the high gas density which influences Faraday rotation measurements of magnetic fields and secondary particle production in hadronic interactions of cosmic ray nuclei with the ambient thermal gas. New estimates of magnetic fields in cooling flow and non-cooling flow clusters are presented, which are based on a newly developed Fourier analysis of extended Faraday rotation maps. We further present new constraints on the cluster cosmic ray proton population using radio and gamma-ray observations measurements of cluster cooling flows, which are especially suited for this purpose due to their high gas and magnetic energy densities. We argue that radio synchrotron emission of cosmic ray electrons generated hadronically by cosmic ray protons is a very plausible explanation for the radio mini-halos observed in some cooling flows.

1. Cooling flows as a window to non-thermal intra-cluster medium components

Cooling flows (CFs) are especially well suited places to find traces of otherwise nearly invisible non-thermal components of the intra-cluster medium (ICM) due to the extreme gas densities observed in CF regions. The faded and therefore invisible remnants of radio galaxy cocoons, so-called *radio ghosts* (Enßlin 1999) or *ghost cavities*, were first detected in CFs by the absence of X-ray emissivity in the ghost's volume in contrast to the highly X-ray luminous cooling flow gas surrounding it (Böhringer et al. 1993; Fabian et al. 2000, and many recent Chandra observations). ICM magnetic fields reveal their presence prominently in CFs by extreme Faraday rotation measures. Cosmic ray electrons (CRe) are seen in CFs by their radio synchrotron radiation in the strong CF magnetic fields. Cosmic ray protons (CRp) in the ICM are most likely to be detected for the first time within CFs via their hadronic interaction with the dense CF gas leading to gamma rays and CRe.

A better knowledge of these non-thermal components of the ICM – especially in the CF regions – is highly desirable, since they play important roles in the heat balance of the gas through heating by CRp, radio ghost buoyant movements, and suppression of heat conduction by magnetic fields. Additionally, such non-thermal components are tracers of the violent dynamics of the ICM and may help to solve some of the puzzles about CFs.

In this article, we present our recent progress in measuring cluster magnetic fields (Sect. 2) and cosmic ray protons (Sect. 3) in cooling flows. We focus on ideas and results, leaving the technical details to the publications given in the reference list.

2. Faraday rotation & magnetic fields

2.1. *Source intrinsic or external?*

The Faraday rotation effect arises whenever polarised radio waves traverse the magnetised ICM which leads to a rotation of the position angle of polarisation. This effect allows the measurement of the (electron density weighted) line of sight component of cluster magnetic fields. Due to projection, it is not clear where between the radio emitting volume (typically a radio galaxy cocoon) and the observer the Faraday rotation occurs (see Fig. 1).

In order to test if the Faraday rotation is produced in a mixing layer between the radio galaxy cocoon and its surrounding ICM, Rudnick & Blundell (2003) compared rotation measure (RM) maps with intrinsic polarisation position angle (PA) maps of the same radio source. The PA is parallel to the source intrinsic magnetic fields and should be uncorrelated to the RM if the Faraday rotation is produced by a source external magnetic field. Therefore, any real co-spatial structures in RM and PA maps would be a very strong indicator of an RM originating from a mixing layer, since only then an RM signature correlated to the PA could be produced. Rudnick & Blundell (2003) tested for such co-spatial structures by measuring the clustering in RM-PA scatter plots and claimed to have found a significant correlation in the RM and PA maps of a radio galaxy.

However, it was shown by Enßlin et al. (2003) that strong clustering in RM-PA scatter plots appears whenever the RM and PA maps have patchy structures independently if the maps are correlated or fully uncorrelated. Such patchy structures are also observed for the maps analysed by Rudnick & Blundell (2003). In order to test without bias for potential co-spatial RM and PA structures, Enßlin et al. (2003) developed a method which relies on the alignment of gradients in the PA and RM maps in a sample of radio galaxy datasets. No large-scale gradient alignments could be measured, however a small-scale gradient alignment is present in all maps. Using a suitable additional test, it could be shown that

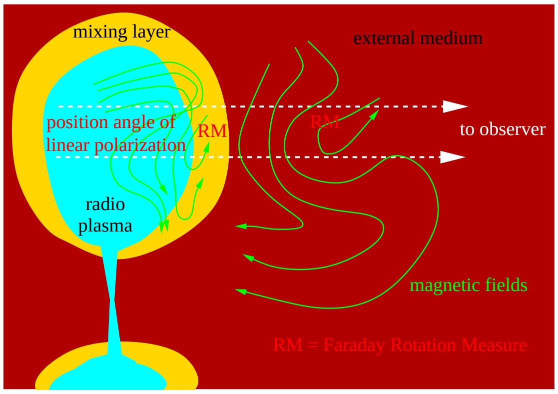

FIG. 1.— Faraday rotation might be generated by source intrinsic or extrinsic magnetic fields. In the first case co-spatial structures in RM and PA are possible, since the RM would be produced in a mixing layer in which the fields carry information about the source intrinsic magnetic field geometry, which determines the PA.

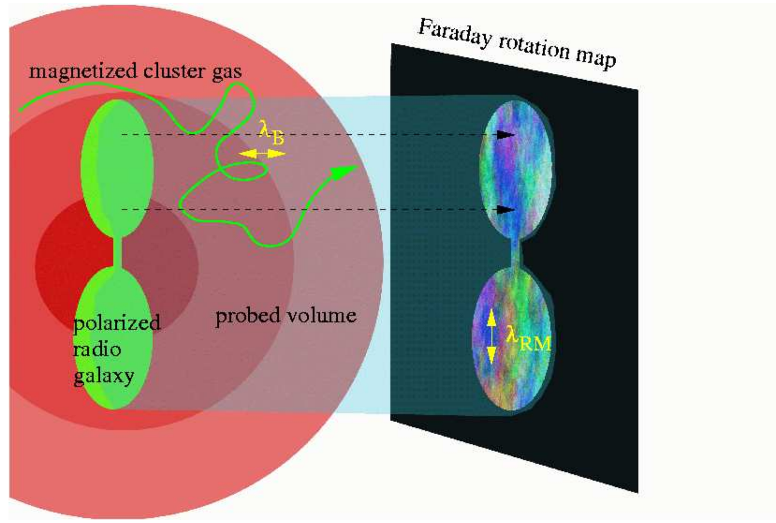

FIG. 2.— Geometry of a Faraday rotation measurement of intracluster magnetic fields. The volume probed for magnetic fields is described by a sampling window function which is non-zero only within the volume in front of the used polarised radio cocoon. The window function values scale with the cluster gas density, modelling the structered sensitivity of the Faraday effect to ICM magnetic fields.

this alignment signal is a residual of correlated imperfections arising in the RM and PA map making process. Such imperfections produce anti-parallel RM and PA gradients – as found to be responsible for the full small-scale alignment signal – whereas real co-spatial structures should produce parallel and anti-parallel gradients with the same probability.

Therefore, currently no evidence exists for Faraday rotation being local to the source. Independently, there is evidence for relatively strong external magnetic fields by diffuse magneto-synchrotron emission from galaxy clusters observed as *radio halos* and *radio relics*. Furthermore, an RM dispersion excess is detected for background radio sources seen through galaxy clusters when compared to control samples (Clarke et al. 2001, and these proceedings). Additionally, given the Laing-Garrington effect (Laing 1988; Garrington et al. 1988), we conclude that the assumption of RM being produced in the foreground ICM of cluster radio sources is strongly favoured. We will adopt this point of view in the following of this article.

2.2. *Statistical analysis of RM maps*

A sketch of the typical geometry in which magnetic fields are measured from Faraday rotation maps is given in Fig. 2. The cluster magnetic field is sampled in a volume - the sampling window function (or window for short), which is shaped by the geometry of the used radio source and the gas distribution of the cluster observed (Enßlin & Vogt 2003). If the window is sufficiently extended, the ICM magnetic field can be regarded to be sampled statistically. This may allow to use statistical methods to restore some of the information lost by the projection of the fields into the RM map.

A crucial information for the measurement of magnetic fields from RM maps is the magnetic autocorrelation length λ_B. If this is known, the central magnetic field strength of the cluster would simply follow from

$$\langle B^2 \rangle = \frac{2\,\langle \mathrm{RM}^2 \rangle}{a_0^2\, n_e^2\, L\, \lambda_B}, \qquad (1)$$

where $\langle \mathrm{RM}^2 \rangle$ is the RM dispersion, L is the depth of the Faraday screen, which is well defined in terms of the window function (Enßlin & Vogt 2003), $a_0 = e^3/(2\pi m_e^2 c^4)$, and n_e is the (central) electron density. Here, it is assumed that the magnetic fields are distributed isotropically, so that the observed line-of-sight magnetic field component is representative also for the other two components.

Unfortunately, the magnetic autocorrelation length λ_B is not directly accessible. However, the RM autocorrelation length λ_{RM} of the RM maps is easily measurable. Although these length scales are often assumed to be equal in the literature, they are two distinct quantities which usually differ. Under typical circumstances λ_{RM} is expected to exceed λ_B. The reason for this is that RM maps are more sensitive to large-scale magnetic structures than to small-scale structures, since the latter's imprint on the RM maps suffers from stronger cancelling effects due to field reversals along the line-of-sight. Therefore, inserting λ_{RM} instead of λ_B into Eq. 1 should lead to an underestimation of the real magnetic field strength.

An approach to circumvent these difficulties is derived by Enßlin & Vogt (2003): under the assumption of a sufficiently large window, and statistically isotropic magnetic fields with vanishing divergence, it can be shown that the 2-dimensional power-spectrum of RM maps is identical to the 3-dimensional magnetic field power-spectrum up to a window function dependent (and therefore known) constant of proportionality. This allows the measurement of the magnetic power-spectrum $\varepsilon_B(k)$ by Fourier transforming RM maps. From the magnetic power spectrum, λ_B and the average (cluster central) magnetic field energy density can be calculated.

2.3. *Confronting theory with data*

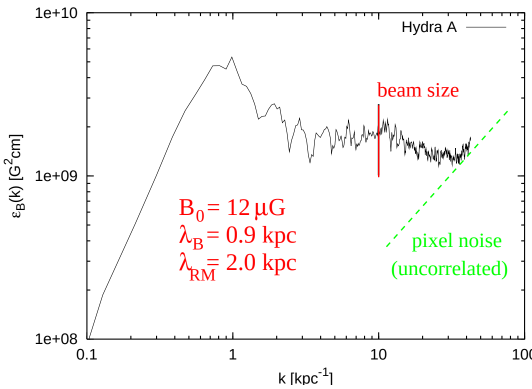

FIG. 3.— 1-dimensional magnetic power spectrum of magnetic fields in the central region of the Hydra cluster. The observational beam size and the spectral slope of uncorrelated sub-beam noise are marked. The estimates of magnetic field strength and length scales are derived by integrating up to the k-vector corresponding to the beam size.

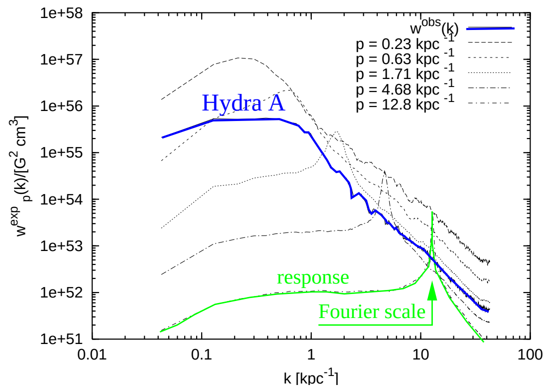

FIG. 4.— Response to single-scale magnetic power spectra. The 3-dimensional magnetic power spectrum $w(k)$ of Hydra A (blue) and the responses of single-scale magnetic power spectra (delta functions located at Fourier-scale p) seen through the window function of Hydra A are shown.

The theoretical formalism of Enßlin & Vogt (2003) was applied to an RM map of the north lobe of Hydra A by Vogt & Enßlin (2003). This polarised radio source is embedded in the Hydra cluster cooling flow region. The window function was modelled using up-to-date electron density profiles of the Hydra cluster from X-ray observations. It was assumed that the northern radio cocoon points towards the observer with an angle of 45°, consistent with the Laing-Garrington effect observed for this source (Taylor & Perley 1993). The resulting power-spectrum is shown in Fig. 3. The cluster central magnetic fields are estimated to have a typical field strength of $12\,\mu$G, if one integrates this power spectrum up to the Fourier k-vector corresponding to the observational resolution (beam size). As predicted, the magnetic autocorrelation length is significantly shorter than the RM autocorrelation length: $\lambda_B = 0.9$ kpc compared to $\lambda_{\rm RM} = 2$ kpc. If $\lambda_{\rm RM}$ had been used instead of λ_B the typical magnetic energy density would have been underestimated by more than a factor of two.

One is tempted to measure the spectral slope of the magnetic power spectrum from Fig. 3 in order to compare it to predictions of magneto-hydrodynamical turbulence. Unfortunately, this is not straightforwardly possible. The difficulties are caused by the finite size of the window through which the magnetic fields are observed. Any finite window in real space leads to a redistribution of power in the Fourier-space. Due to the small size of the window and its complicated shape, this effect is significant and has to be taken into consideration. A possibility to investigate this effect is to calculate theoretically the expected response of the measured power spectrum to single-scale (isotropic) magnetic fluctuations seen through the window.

The results of such calculations are displayed in Fig. 4. The response to magnetic power on large Fourier-scales, and therefore to small-scale spatial power, resembles the delta-function. However, magnetic large scale-power is strongly redistributed over the full Fourier-space. Since the large-scale power dominates the total power, the intrinsic spectrum of the magnetic fields in the Hydra A cluster are masked by this effect. Experiments with power-law spectra observed through the window reveale that the observational data is consistent with Kolmogorov-like or steeper spectra.

The redistribution of power in Fourier space affects the accuracy of magnetic field estimates. Since the estimated magnetic field strengths are an integral quantity of the power-spectra, the redistribution of power within the Fourier space typically introduces only a moderate error. Magnetic field estimates seem to be robust to this effect, at least on the few 10 % accuracy level.

2.4. *Improving data: Pacman*

Usually, the RM is determined using a least square fit in order to solve $\Phi = \mathrm{RM}\,\lambda^2 + \mathrm{PA}$, where Φ is the measured position angle of polarisation at the observed wavelength λ. However, Φ is observationally only constrained to values between 0 and π leaving the freedom of additions of $\pm n\pi$ (where n is an integer) causing the so called $n\pi$ ambiguity. Therefore, the least square fit has to be applied to all possible $n\pi$-combinations while searching for the $n\pi$-combination for which χ^2 is minimal.

Traditionally, the minimisation of χ^2 is done for each data pixel separately. In these RM maps, steps in the RM value from one pixel to the other could be observed. These steps are mostly detected for noisy regions. They seem to be artificial and due to a false solution of the $n\pi$-ambiguity. Enßlin & Vogt (2003) showed that artefacts in the RM map can lead to flattening of the power spectra in their analysis. Thus, magnetic field strengths estimate are likely to be overestimated.

In order to determine RM values more reliably, Dolag et al. (in prep.) suggest to use non-local information to solve the $n\pi$-ambiguity. The new *Pacman* algorithm takes advantage of smooth regions in Φ. For such smooth regions for all observed wavelengths, the RM distribution is expected to be also smooth and is not expected to show jump or step like features. Therefore, the solution to the $n\pi$-ambiguity can be applied to this whole region. This

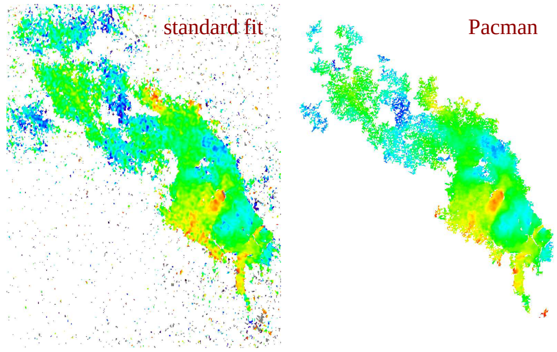

FIG. 5.— A comparison between an RM map obtained using standard least square fit routines on the left to an RM map produced by *Pacman* on the right hand side is shown. A by-eye-comparison reveals that the *Pacman* map is smoother.

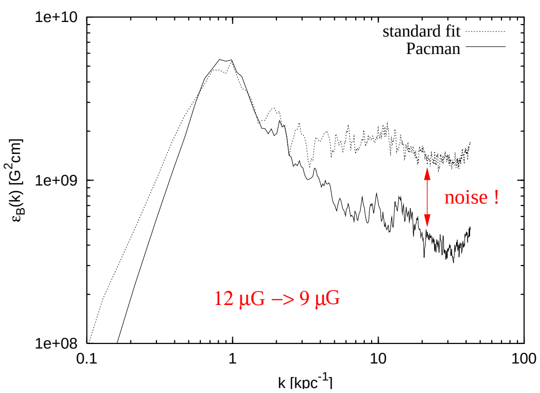

FIG. 6.— The 1-dimensional power spectra calculated for the *Pacman* map is represented by the solid line in comparison to the dashed line which was derived by analysing the standard fit RM map. The influence of the map making process is clearly visible.

has the advantage that noisier areas can profit from leass noisy areas.

The application of *Pacman* can lead to a drastic decrease of noise in RM maps as can be seen in Fig. 5. In this figure an RM map which is obtained using standard least square fit algorithm is shown on the left side. In comparison to it an RM map generated by *Pacman* is exhibited on the right hand side. Already a visual inspection of this figure reveals that the *Pacman* map is smoother than the standard fit map.

If one repeats the analysis described above and derives the magnetic power spectra for the *Pacman* map as shown in Fig. 6, one can see the effect of noise in the RM map. The power spectra for the *Pacman* map is steeper and thus, leads to a lower estimate for the central magnetic field strength of the order of about $\sim 9\ \mu$G.

3. Hadronic interactions of cosmic ray protons

3.1. *Hadronic reactions*

Approximately once in a Hubble time a cosmic ray proton (CRp) collides inelastically with a nucleon of the ICM gas of non-cooling flow clusters. Within CFs, such collisions are much more frequent due to the higher target densities. Such inelastic proton (p) nucleon (N) collisions hadronically produce secondary particles like relativistic

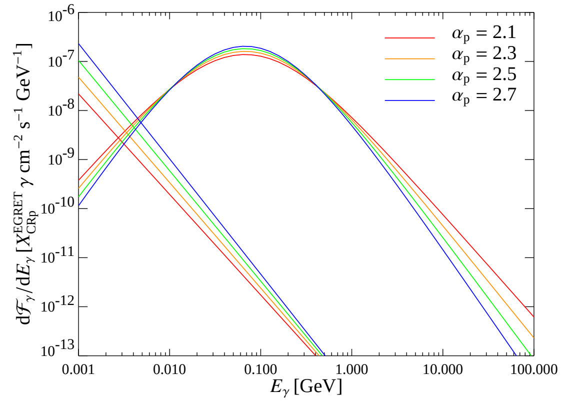

FIG. 7.— Theoretical gamma-ray spectra of the Perseus cluster resulting from CRp hadronic interactions with the CF gas. The assumed CRp spectra are normalised to be marginally consistent with the EGRET $E_\gamma > 100$ MeV non-detection limits. Results for different proton spectral indices are shown. The π^0 decay bump is clearly visible. The low energy part of the spectra is populated by secondary CRe inverse Compton scattering cosmic microwave background photons into the gamma-ray regime. The CRe population was calculated neglecting synchrotron radiation energy losses. Thus, realistic inverse Compton spectra due to this process will exhibit a lower normalisation than displayed here.

electrons, positrons, neutrinos and gamma-rays according to the following reaction chain:

$$
\begin{aligned}
& p + N \rightarrow 2N + \pi^{\pm/0} \\
& \quad \pi^{\pm} \rightarrow \mu^{\pm} + \nu_\mu/\bar{\nu}_\mu \rightarrow e^{\pm} + \nu_e/\bar{\nu}_e + \nu_\mu + \bar{\nu}_\mu \\
& \quad \pi^0 \rightarrow 2\gamma\,.
\end{aligned}
$$

The resulting gamma-rays can be detected directly with current and future gamma-ray telescopes. The relativistic electrons and positrons (summarised as CRe) are visible due to two radiation processes: inverse Compton scattering of background photon fields (mainly the cosmic microwave background, but also starlight photons) and radio synchrotron emission in ICM magnetic fields. Especially the latter process provides a very sensitive observational signature of the presence of CRp in cooling flows not only because of the tremendous collecting area of radio telescopes, but also due to the strong magnetic fields in CFs, as Faraday rotation measurements demonstrate.

3.2. *Gamma ray constraints from EGRET*

Assuming that the CRp population can be described by a power law distribution in momentum, Pfrommer & Enßlin (2003a) developed an analytical formalism to describe the secondary emission spectra from hadronic CRp interactions which exhibit the simplicity of textbook formulae. This formalism was applied to a sample of nearby X-ray luminous galaxy clusters which are also believed to be powerful gamma ray emitters owing to the present high target densities. Synthetic gamma-ray spectra of the Perseus cooling flow cluster calculated using this formalism are shown in Fig. 7. Assuming that the CRp population follows the spatial distribution of the thermal ambient intra-cluster gas, we can define the

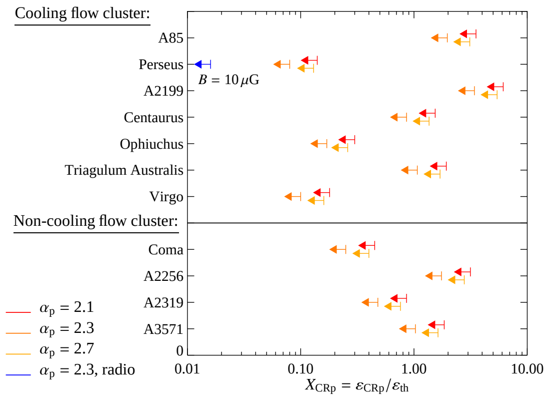

FIG. 8.— EGRET gamma-ray constraints on the (central) CRp energy density ($\varepsilon_{\rm CRp}$, for various CRp spectral indices) in terms of the cluster central thermal energy density ($\varepsilon_{\rm th}$) for CF and non-CF clusters. The constraint from the Perseus cluster radio mini-halo observation is also displayed while assuming a typical CF cluster magnetic field strength (blue arrow). If radio mini-halos are entirely produced hadronically by CRp then the constraint derived for the Perseus cluster is an actual measurement for $X_{\rm CRp}$ and not only an upper limit.

CRp scaling ratio

$$X_{\rm CRp} \equiv \frac{\varepsilon_{\rm CRp}}{\varepsilon_{\rm th}}. \tag{2}$$

The parent CRp spectra giving rise to the hadronically induced gamma-ray spectra are normalised to upper limits on the gamma ray emission obtained by EGRET observations for energies $E_\gamma > 100$ MeV. For nearby CF clusters, this analysis constrains CRp energy densities relative to the thermal energy density to $X_{\rm CRp} \sim 10\%$. The real gamma ray spectrum of Perseus is not expected to be far below these spectra. Many processes like supernova driven galactic winds, structure formation shock waves, radio galaxy activity and in-situ turbulent particle acceleration support this expectation. These processes should have produced a CRp population characterised by an energy density relative to the thermal energy density of at least a few percent.

The EGRET gamma ray observation of Perseus limits the CRp content in the central region to be below $X_{\rm CRp} \sim 10\%$. For the full sample of nearby X-ray luminous clusters upper limits of the same order of magnitude were obtained as can be seen in Fig. 8. It is obvious from this compilation that CF clusters are extremely well suited to visualise even small CRp populations.

3.3. *Gamma rays from the central CF region of the Virgo cluster*

Recently the HEGRA collaboration (Aharonian et al. 2003) announced a TeV gamma ray detection from the giant elliptical galaxy M 87 which is situated at the centre of the CF region of the Virgo cluster. Using imaging atmospheric Čerenkov techniques, this gamma ray detection was obtained at a 4-σ significance level. On the basis of their limited event statistics, it is inconclusive whether the detected emission originates from a point source or an extended source. Despite testing for eruptive behaviour of M 87, no time variation of the TeV gamma ray flux has been found.

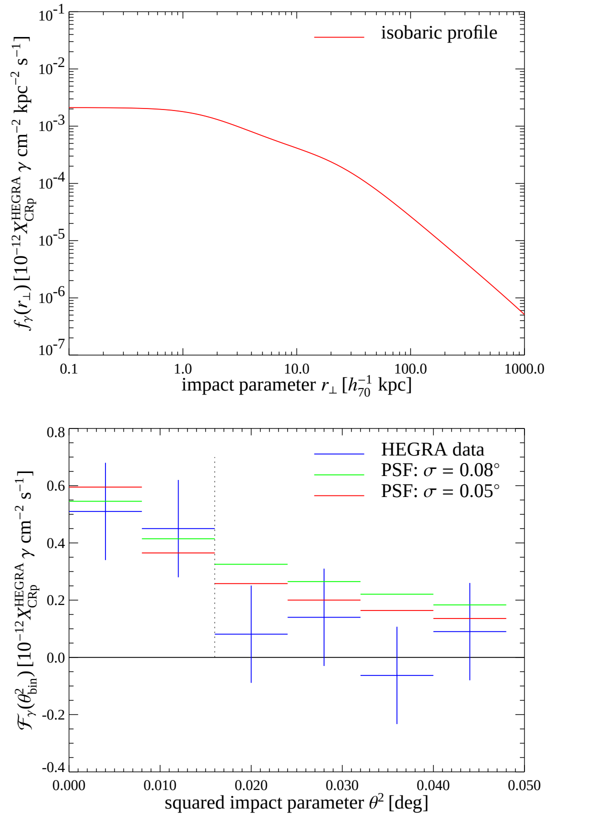

FIG. 9.— **Upper panel:** Modelled γ-ray surface flux profile of the CF region within the Virgo cluster. The profile is normalised by comparing the integrated γ-ray flux above 730 GeV to HEGRA data of M 87 within the innermost two data points. **Lower panel:** Comparison of detected to predicted γ-ray flux within the central aperture and the innermost annuli for two different widths of the PSF. The red lines correspond to an optimistic PSF of $\sigma = 0.05°$ whereas the green lines are calculated for a conservative $\sigma = 0.08°$ for a soft gamma ray spectrum. The vertical dashed line separates the data from the noise level at a position corresponding to $r_\perp = 37.5$ kpc.

Pfrommer & Enßlin (2003b) applied the previously described analytical formalism (Sect. 3.2) of secondary gamma ray emission spectra resulting from hadronic CRp interactions to the central CF region of the Virgo cluster. While combining the observed TeV gamma ray emission to EGRET upper limits, they constrain the CRp spectral index $\alpha_{\rm GeV}^{\rm TeV} < 2.3$ provided the γ-ray emission is of hadronic origin and the population is described by a single power-law ranging from the GeV to TeV energy regime.

A comparison of the observed to the predicted gamma ray emissivity profiles is shown in Fig. 9. In order to allow for finite resolution of the Čerenkov telescope, the real profile was convolved with the point spread function (PSF) of the HEGRA instrument. The more optimistic PSF of $\sigma = 0.05°$ for harder gamma ray spectra being favoured by our model as well as the conservative choice of a PSF derived from softer Crab-like spectra are both consistent with the observed data. When considering an

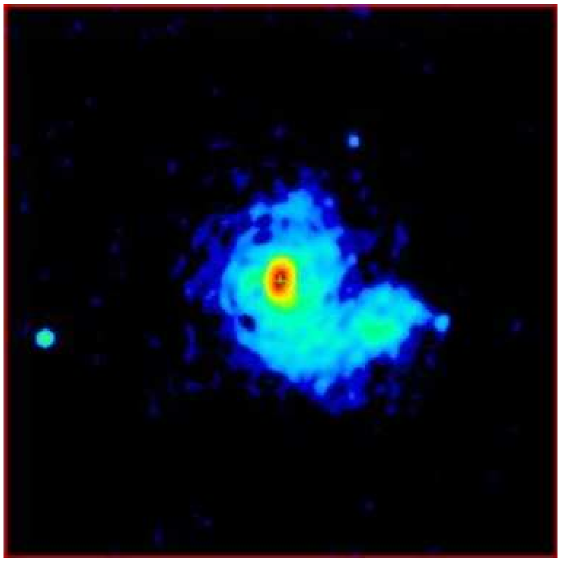

FIG. 10.— The Perseus radio mini-halo at 1.4 GHz from Pedlar et al. (1990) with an extent of $160h_{70}^{-1}$ kpc in diameter. At the very centre is an extremely bright flat-spectrum core owing to relativistic outflows of the radio galaxy NGC 1275. This outflow was subtracted from this image to make the extended structure more visible. The position of the radio galaxy is marked by the green cross in the centre of the red region.

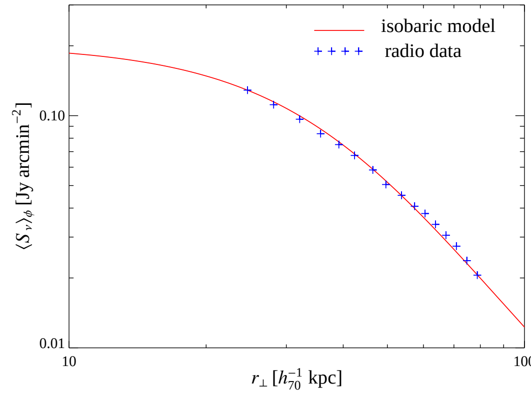

FIG. 11.— Radio emissivity profile of the Perseus mini-halo at 1.4 GHz observed by Pedlar et al. (1990) (crosses) and predicted due to hadronic interactions of CRp by Pfrommer & Enßlin (2003a). Both the required CRp scaling ratio $X_{\rm CRp} \simeq 2\%$ and the morphological match of the observed and predicted radio emissivities strongly indicate the hadronic origin of radio mini-halos.

aged CRp population which has already suffered from significant Coulomb losses, CRp scaling ratios of the order of $X_{\rm CRp} \sim 50\%$ are obtained for the innermost region of Virgo within $r_\perp = 37.5$ kpc.

Since the emission region is dominated by the giant radio galaxy M 87, other mechanisms like processed radiation of the relativistic outflow or dark matter annihilation could also give rise to the observed gamma ray emission. Nevertheless, the hadronic scenario probes the CRp population within a mixture of the inter stellar medium of M 87 and the ICM of the Virgo CF region yielding either an upper limit or a detection on the CRp population, provided this scenario applies.

3.4. *Radio mini-halos*

An upper limit to the CRp population of $X_{\rm CRp} \simeq 2\%$ which is derived from radio observations of the Perseus galaxy cluster is displayed in Fig. 8. The radio emissivity of hadronically generated CRe depends on the assumed magnetic field strength. Thus, upper limits on $X_{\rm CRp}$ rely on the same assumption. However, in the case of strong magnetic fields (above $3\,\mu$G), the dependence of $X_{\rm CRp}$ on the assumed field strength is very weak, since synchrotron losses dominate in this regime. If radio mini-halos are entirely produced hadronically by CRp then the constraint derived for the Perseus cluster is an actual measurement for $X_{\rm CRp}$ and not only an upper limit.

The Perseus radio mini-halo at 1.4 GHz is shown in Fig. 10 as observed by Pedlar et al. (1990). The emission due to the relativistic jet has been subtracted to make the extended structure more visible. The spatial extent of the radio mini-halo of $160h_{70}^{-1}$ kpc in diameter is too large to be accounted for by synchrotron emission of direct accelerated CRe in structure formation or accretion shocks. Thus one needs to consider other injection processes of CRe into the ICM which are responsible for the observed diffuse radio emission. Besides the reacceleration scenario of mildly relativistic CRe ($\gamma \simeq 100 - 300$) which are accelerated in-situ by turbulent Alvén waves (Gitti et al. 2002, and these proceedings), the hadronic injection scenario of CRe is a promising alternative.

Azimuthally averaging the radio emission shown in Fig. 10 yields the radio emissivity profile as displayed in Fig. 11. For a comparison, we overlaid synthetic radio surface brightness profiles resulting from the hadronic scenario. There is a perfect morphological match between observed and predicted profiles. Alongside the comparably small number of CRp required to account for the observed radio mini-halo, this suggests a hadronic origin of the radio mini-halo in Perseus.

4. **Non-thermal conclusions**

Our results on magnetic fields and cosmic rays in galaxy cluster cooling flows can be summarised as follows:

Magnetic fields in cooling flows

- Sophisticated statistical tests on Faraday rotation maps as suggested by Rudnick & Blundell (2003) reveal no indications that the Faraday effect occurs in the vicinity of the polarised radio source observed (Enßlin et al. 2003). Additional several independent pieces of evidence in favour of strong intra-cluster magnetic fields lead us therefore to believe that the Faraday rotation signal is due to intracluster fields, and that the effect is not generated in a hypothetical mixing layer surrounding the observed radio source.

- Faraday rotation measure maps provide a window through which we get a glimpse on the turbulent magnetised intra-cluster medium. However, they give us only a projected and partial view of the cluster magnetic field configuration. Therefore statistical methods have to be used to decipher the Faraday signal in terms of magnetic field properties.

- The magnetic field strength derived from the dispersion of rotation measure values depends critically – besides geometrical factors of the galaxy cluster – on the magnetic autocorrelation length, which is not identical to and usually shorter than the autocorrelation length of the rotation measure fluctuations. However, both can be measured from such maps with a novel analysis method (Enßlin & Vogt 2003).

- An application of the novel analysis method of Faraday rotation map to data of a Hydra A reveals magnetic fields $\sim 12\,\mu$G in the centre of the cooling flow of the Hydra cluster (Vogt & Enßlin 2003). The magnetic autocorrelation length is 0.9 kpc, and therefore shorter than the rotation measure autocorrelation length of 2.0 kpc, as expected. The magnetic power-spectrum is consistent with a Kolmogorov-like or steeper spectrum.

- The small-scale fluctuations in the Faraday rotation map of Hydra A are dominated by noise. The southern maps reveal several step-function-like artefacts which is probably due to the ambiguity in the absolute polarisation angle used to determine the rotation measure. In order to improve the map quality a new map generating algorithm is currently being developed – *Pacman* – which uses non-local information in order to solve angle ambiguities and which uses improved fitting methods. A preliminary version of *Pacman* produces maps with strongly reduced noise level.

Cosmic ray protons in cooling flows

- We argue that cooling flows of galaxy clusters are well suited to reveal or constrain any cosmic ray proton population via radiation from hadronic interactions with the ambient gas nuclei. Such collisions lead to gamma-rays and cosmic ray electrons. The former would have been seen above 100 MeV by the EGRET telescope if the cosmic ray protons had energy densities relative to the thermal gas exceeding 10% (Pfrommer & Enßlin 2003a).

- The giant elliptical galaxy M 87 in the centre of the Virgo cluster cooling flow region has recently been detected at TeV energies by the HEGRA instrument (Aharonian et al. 2003). These gamma rays could be produced by hadronic interactions of a cosmic ray proton population if its spectral index $\alpha_{\rm GeV}^{\rm TeV} < 2.3$ and its energy density is of the order of 50% of the gas within the transition/mixture of inter-stellar and intra-cluster medium within M 87 (Pfrommer & Enßlin 2003b).

- Cosmic ray electrons produced in hadronic interactions are a very sensitive indicator of cosmic ray protons due to their strong emissivity. Radio synchrotron emission of such electrons in strong cooling flow magnetic fields of $\sim 10\,\mu$G limit the cosmic ray proton energy density to $\sim 2\%$ or less compared to the thermal one in the Perseus cluster cooling flow (Pfrommer & Enßlin 2003a).

- Diffuse radio emission from the Perseus cluster cooling flow was detected – the so called Perseus *radio mini-halo*. This radio synchrotron emission may be induced by CRp interactions in the ICM. This scenario is strongly supported by the very moderate energy requirements (2% of the thermal energy) and the excellent agreement between the observed and the theoretically predicted radio surface profile (Pfrommer & Enßlin 2003a).

We thank Tracy Clarke, Klaus Dolag, Greg Taylor, Francesco Miniati, and Sebastian Heinz for discussion and collaboration, Alan Pedlar for the permission to reproduce the Perseus mini-halo image, and the conference organisers for an excellent meeting.

References

Aharonian, F., Akhperjanian, A., & Beilicke, M. *et al.*. 2003, A&A, 403, L1
Böhringer, H., Voges, W., Fabian, A. C., Edge, A. C., & Neumann, D. M. 1993, MNRAS, 264, L25
Clarke, T. E., Kronberg, P. P., & Böhringer, H. 2001, ApJ, 547, L111
Enßlin, T. A. 1999, in Diffuse Thermal and Relativistic Plasma in Galaxy Clusters, 275, astro-ph/9906212
Enßlin, T. A. & Vogt, C. 2003, A&A, 401, 835
Enßlin, T. A., Vogt, C., Clarke, T. E., & Taylor, G. B. 2003, ApJ, in press, astro-ph/0301552
Fabian, A. C., Sanders, J. S., Ettori, S., Taylor, G. B., Allen, S. W., Crawford, C. S., Iwasawa, K., Johnstone, R. M., & Ogle, P. M. 2000, MNRAS, 318, L65
Garrington, S. T., Leahy, J. P., Conway, R. G., & Laing, R. A. 1988, Nature, 331, 147
Gitti, M., Brunetti, G., & Setti, G. 2002, A&A, 386, 456
Laing, R. A. 1988, Nature, 331, 149
Pedlar, A., Ghataure, H. S., Davies, R. D., Harrison, B. A., Perley, R., Crane, P. C., & Unger, S. W. 1990, MNRAS, 246, 477
Pfrommer, C. & Enßlin, T. A. 2003a, A&A, in press, astro-ph/0306257
—. 2003b, A&A, 407, L73
Rudnick, L. & Blundell, K. M. 2003, ApJ, 588, 143
Taylor, G. B. & Perley, R. A. 1993, ApJ, 416, 554
Vogt, C. & Enßlin, T. A. 2003, A&A, in press, astro-ph/0309441